ResearchGate

See discussions, stats, and author profiles for this publication at: https://www.researchgate.net/publication/257806346

Kinetic study of photodegradation of water soluble polymers

ARTICLE *in* IRANIAN POLYMER JOURNAL · DECEMBER 2012

Impact Factor: 1.81 · DOI: 10.1007/s13726-012-0091-5

CITATIONS
8

READS
46

3 AUTHORS:

Samira Ghafoori
Ryerson University
22 PUBLICATIONS **73** CITATIONS
SEE PROFILE

Mehrab Mehrvar
Ryerson University
99 PUBLICATIONS **1,121** CITATIONS
SEE PROFILE

Philip K. Chan
Ryerson University
18 PUBLICATIONS **223** CITATIONS
SEE PROFILE

Available from: Samira Ghafoori
Retrieved on: 25 January 2016

I&EC research
Industrial & Engineering Chemistry Research

Article

pubs.acs.org/IECR

Free-Radical-Induced Degradation of Aqueous Polyethylene Oxide by UV/H_2O_2: Experimental Design, Reaction Mechanisms, and Kinetic Modeling

Samira Ghafoori, Mehrab Mehrvar,* and Philip K. Chan

Department of Chemical Engineering, Ryerson University, 350 Victoria Street, Toronto, Ontario, Canada, M5B 2K3

ABSTRACT: The advanced oxidation of aqueous polyethylene oxide (PEO) is studied using the UV/H_2O_2 process in a batch recirculation photoreactor. The response surface methodology (RSM), combined with quadratic programming, is used for the experimental design, statistical analysis, and optimization of the process. In the second part, a detailed mathematical model is developed to predict the total organic carbon (TOC) removal as a function of time. Continuous distribution kinetics is applied to establish the kinetic model for the photodegradation of PEO. The model is validated at different influential operating conditions using experimental data obtained by a recirculating batch photoreactor. An excellent agreement between the model predictions and the experimental data is confirmed for all experimental conditions. Also, the intrinsic rate constants are estimated using an optimization algorithm. The model provides a good insight into the free-radical-induced degradation mechanisms and kinetics that could be considered for the process optimization.

1. INTRODUCTION

Synthetic water-soluble polymers are produced in large volumes. Because of their solubility in water, they are widely used in a variety of industrial products and applications, including surfactants, pharmaceuticals, paints, adhesives, paper coating agents, textiles, and detergents.[1] Some of the key functionalities of these substances are their ability to increase the viscosity of solutions, form physical gels, stabilize dispersions and emulsions, induce particle aggregation, and solubilize hydrophobic compounds.[2] Most synthetic water-soluble polymers from industrial effluents are discarded into aqueous environment. Therefore, they can reach conventional sewage disposal systems and subsequently contaminate water resources. In fact, they are not readily biodegradable by the type of microorganism that normally attack most other forms of organic matter and render them to the biological life cycle.[3] Some of the environmental impacts of the synthetic water-soluble polymers are as follows: recalcitrant without significant change in the environment, toxic to soil microbial population and animals, depleting the soil fertility, and carrying heavy metals through the environment.[4] On the other hand, because of their water solubility, they have received less attention in the general public, in comparison to packaging plastics, which are visibly discarded in the environment. Hence, the contribution of this type of polymers to the ever-increasing problem of water pollution is a major concern and their water solubility makes their environmental fate less obvious.[5] Also, most of the techniques currently applied to degrade these types of polymers have been determined to be either inefficient or hazardous to the environment.[6] Therefore, the possibility of degrading these materials to harmless and biologically useful chemical compounds is a challenging task.

In recent decades, advanced oxidation technologies (AOTs) have been applied successfully to degrade recalcitrant pollutants in wastewater.[7−13] AOTs involve the use of UV radiation, O_3, H_2O_2, photocatalysts such as TiO_2, metal catalysts such as Fe ions in the Fenton process, or any combination thereof to generate short-lived nonselective chemical species of high oxidation potential.[14] Free-radical species, especially hydroxyl radicals, mediate fast degradation or decomposition of target organic compounds. In fact, the oxidation potential of these short-lived free radicals is greater than the rest of the oxidants in conventional chemical treatments.[15] AOTs render contaminants to less-toxic intermediates that can be accessible to the efficient biological treatment.[16−18] The unique feature of AOTs in wastewater treatment is that, in most of the processes, they do not generate waste sludge or volatile organic compounds associated with most conventional treatment processes. Among AOTs, the UV/H_2O_2 process has a relatively higher oxidation rate and more simplicity in application and operation, in comparison to other AOTs.[18−20] AOTs are multifactor systems that various parameters such as concentration of organic materials, light intensity, oxidant dosage, reaction time, pH, and other operating conditions influence the efficiency of the system. Therefore, in addition to the single-factor effects, cross-factor effects must be taken into consideration in order to characterize the behavior of such systems. Using experimental design, the identification of factors influencing the multivariable system is conceivable. On the other hand, the information in studying the reaction mechanisms and detailed kinetic modeling of AOTs involving all free radicals and molecular species for the degradation of aqueous soluble polymers is scarce in the open literature.[21,22] Also, most of the established investigations in polymer degradation kinetics have centered on determining the rate of change of average molecular weight.[22−24] Therefore, there is little information available in the open literature in studying the degradation kinetics of

Received: March 6, 2012
Revised: October 23, 2012
Accepted: October 23, 2012
Published: November 7, 2012

ACS Publications © 2012 American Chemical Society

dx.doi.org/10.1021/ie3005995 | *Ind. Eng. Chem. Res.* 2012, 51, 14980−14993

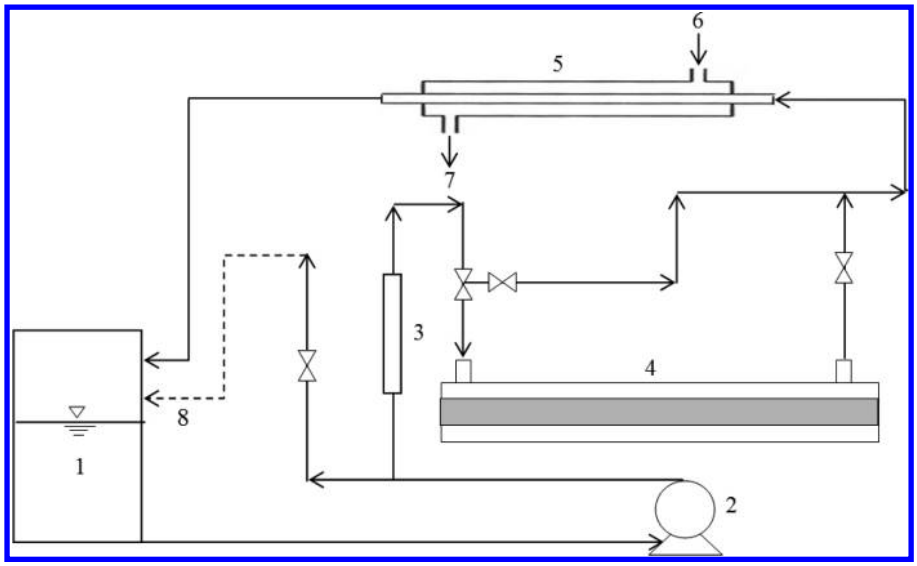

Figure 1. Schematic diagram of the photoreactor setup. Legend: (1) reservoir and collection tank, (2) centrifugal pump, (3) flow meter, (4) UV−C photoreactor, (5) heat exchanger, (6) cooling water inlet, (7) cooling water outlet, and (8) bypass.

soluble polymers using lumped parameters such as chemical oxygen demand (COD) and total organic carbon (TOC). Few studies have considered TOC as an output variable in the kinetic models for some components other than polymers.[25,26]

In the first part of this study, an experimental design was used to investigate the photochemical degradation of a synthetic water-soluble polymer (PEO) by UV/H_2O_2 process. PEO is not amenable to biodegradation. Also, the effects of initial concentrations of PEO and H_2O_2, pH, and recirculation rate on the photodegradation of aqueous PEO by UV/H_2O_2 process were investigated. The optimal values of parameters were determined by means of four-factor five-level central composite design (CCD), combined with response surface methodology (RSM) and quadratic programming. In the second part of this study, a mathematical model was developed to predict the percent TOC removal as the output variable with time in the UV/H_2O_2 process. Continuous distribution kinetics that describes the dynamics of polymer reactions was applied to establish the TOC-based kinetic modeling of the process. The developed model relies on the experimental data achieved in this work, as well as the published data on the rate constants of the reaction between intermediates and hydroxyl radicals. Ultimately, the model was validated by another set of experimental data carried out under different operating conditions, based on the results of the experimental design. Also, the intrinsic rate constants were estimated using an optimization algorithm.

2. MATERIALS AND METHODS

2.1. Materials. PEO with an average molecular weight of 2 × 10^5 g mol^{-1} and H_2O_2 (50% (w/w)) were obtained from Sigma−Aldrich. PEO was used as received and H_2O_2 was diluted to 30% (w/w). NaOH (99%) and H_2SO_4 (99%), both from EMD, were used for pH adjustments.

2.2. Experimental Setup and Procedure. In order to determine the kinetic parameters, a laboratory-scale batch recirculation photoreactor system with uniform light distribution was used. The reactor configuration enables a simple mathematical representation for both mass and radiation balances. A small annular photoreactor (SL-LAB, Siemens Inc.) with the annular space of 1.33 cm was used as part of the recycle system including a centrifugal magnetic pump (Model RK-72012−10, Cole−Parmer), an all-glass heat exchanger (for controlling temperature), and a large volume tank with provisions for sampling and temperature measurements, as shown in Figure 1. The system was also equipped with a bypass valve to control the flow rate and to provide a relief to the pump pressure. The UV lamp (model LP4130, Siemens, Inc.) sealed with the quartz sleeve was positioned at the centerline of the photoreactor with stainless steel housing. This particular geometry (very small annular space) and the method of irradiation lead to have a good approximation of an isoactinic condition (i.e., uniform light distribution) in the photoreactor.[27] The description and operating conditions of the laboratory-scale photoreactor are given in Table 1. The pH was adjusted at the beginning of each experiment by adding few drops of 1 N NaOH or H_2SO_4 as needed and it was measured by a portable pH meter (230A plus, Thermo Orion). No further pH adjustment was made during the experiments.

Table 1. Laboratory-Scale Photoreactor Description and Operating Conditions

item	specification
photoreactor	
type	batch recirculation
inner diameter	2.44 cm
outer diameter	5.11 cm
length	30.5 cm
volume	0.46 L
tank volume	5 L
operating flow rate	0.5−8.5 L min^{-1}
Reynolds number, *Re*	132−2252
lamp	
type	LP Hg UV-14 W
wavelength	254 nm
length	20.5 cm
output power	4 W
temperature	22 °C
pressure	1 atm

dx.doi.org/10.1021/ie3005995 | *Ind. Eng. Chem. Res.* 2012, 51, 14980−14993

The following protocol was pursued in conducting each experiment: PEO solution was prepared by gradually dissolving PEO in a 300-mL beaker containing distilled water with a magnetic stirring bar at 50 °C in order to avoid any foam formation. The solution was then diluted to achieve the desired PEO concentration in a 5-L solution and desired amount of H_2O_2 was added to the solution at the beginning of each experiment. The UV lamp was then turned on for 30 min before the beginning of each experiment to stabilize the light intensity and to degrade any possible organic background or microcontaminant, such as natural organic matter. The solution was fed to the system and the temperature was kept constant at 22 °C during each experiment by means of a heat exchanger. The samples were taken from the collection tank. The TOC concentration of the samples was monitored by a TOC analyzer (Apollo 9000, Teledyne Tekmar, USA). A UV/visible spectrophotometer (Ultrospec 1100 pro) was used to determine the extinction coefficient of PEO.

3. EXPERIMENTAL DESIGN AND OPTIMIZATION STUDIES BY RSM

The RSM design, which is a combination of mathematical and statistical techniques, reduces the number of experiments in comparison to that of a full experimental design.[28] The RSM is able to optimize the operating conditions in multifactor systems by considering the interactions among variables.[29] Therefore, with minimum number of experiments, an optimal response could be achieved. There are usually three steps in the RSM:

- design,
- response surface modeling via regression at desired values of the process response, and
- optimization to find the best operating conditions.

In the present study, a four-factor, five-level central composite design (CCD), combined with RSM and quadratic programming, were used to maximize the percent TOC removal as the process response. The CCD is considered as the most successful factorial design.[30] In general, the quadratic programming is a linearly constrained optimization problem with a quadratic objective function. The initial concentration of PEO (X_1), the initial concentration of H_2O_2 (X_2), pH (X_3), and the recirculation rate (X_4) were the four independent variables studied. The percent TOC removal was considered as the dependent factor (process response). The variables were coded at five levels between −2 and +2, as shown in Table 2. The critical ranges of the factors were selected based on a set of preliminary experiments.

Data from CCD were subjected to the following quadratic equation model to predict the system response and estimate the coefficients by the least-squares regression:

Table 2. Independent Variables and Their Coded Levels Based on CCD

independent variables	symbols	coded levels				
		−2	−1	0	1	2
initial concentration of PEO (mg L^{-1})	X_1	10	20	30	40	50
initial concentration of H_2O_2 (mg L^{-1})	X_2	300	500	700	900	1100
pH	X_3	3	5	7	9	11
recirculation rate (L min^{-1})	X_4	0.5	2.5	4.5	6.5	8.5

$$Y = \beta_0 + \sum_{i=1}^{k} \beta_i X_i + \sum_{i=1}^{k} \beta_{ii} X_i^2 + \sum_{i=1}^{k-1} \sum_{j=2}^{k} \beta_{ij} X_i X_j + e \quad (1)$$

where Y is the predicted response, β_0 is the constant coefficient (intercept term), β_i represents the linear coefficients, β_{ii} are the quadratic coefficients, and β_{ij} represents the interaction coefficients. The parameters X_i and X_j are independent variables, where k and e are the number of factors (in this case, k = 4) and the residual term allowing uncertainties between observed and predicted values, respectively. A statistical software, Design-Expert 8.0.5 (trial version), was used for the regression analysis and the coefficient estimation of the response function. The statistical significance of the model equation was analyzed by the analysis of variance (ANOVA). Three-dimensional (3D) surface and two-dimensional (2D) contour plots were developed while holding a variable constant in the quadratic model. The experimental and predicted values were compared to validate the model. The optimal operating conditions to maximize the percent TOC removal were also determined using a numerical technique built in the software.

4. REACTION MECHANISM AND KINETIC MODELING

The reaction scheme for the photodegradation of PEO by the UV/H_2O_2 process is summarized in Table 3. All reaction mechanisms are based on extensively accepted photochemical reactions and the rate constants in advanced oxidation processes (Reactions R1−R13). The complete mineralization of the PEO monomer to H_2O and CO_2, disregarding other intermediates, is presented in Reactions R14−R16. A kinetic model based on the mass balance of species of interest in the reaction steps proposed in Table 3 was developed. The kinetic model predicts the TOC concentration profile of the polymer as a function of time. The model assumptions are as follows:

- The pH is considered constant, since it has been proven that changes in pH during the process have no significant effect on the model predictions;[31]
- The photon absorption by PEO does not show any TOC removal, indicating that the quantum yield in the direct photolysis of PEO (PEO $\xrightarrow{h\nu,\varphi_{TOC}}$?) is zero, i.e., $\varphi_{TOC} = 0$;
- Only hydroxyl radical attack is responsible for the polymer degradation, because the oxidation potential of other radicals is negligible, compared to that of hydroxyl radicals;[32]
- H_2O_2 and HO_2^-, acid−base conjugates, are the main light-absorbing species;
- Oxidation intermediates of PEO other than ethylene oxide (monomer) are not considered in the rate expressions; and
- Unlike most kinetic modeling approaches, unsteady-state assumptions are used in the free-radical rate expressions to have a better prediction of the degradation in the completely mixed recirculation batch system.

The kinetic modeling of the polymer photodegradation (Reactions R14−R16) in an aqueous solution requires more attention, since the degradation of polydisperse high-molecular-weight materials results in the formation of thousands of polymeric chains with different chain lengths and various chemical compositions, i.e., the number of branches, the presence and the position of a radical center, and the location of double bonds. Tracking each of these distinct species individually is prohibitive and, because of current hardware

dx.doi.org/10.1021/ie3005995 | Ind. Eng. Chem. Res. 2012, 51, 14980−14993

Table 3. Reaction Mechanisms for Complete Mineralization of PEO by UV/H_2O_2 Process

reaction	reaction	rate constant	ref
R1	$H_2O_2 \xrightarrow{\varphi_{H_2O_2}, h\nu} 2^{\bullet}OH$	0.5 mol Einstein^{-1}	31
R2	$^{\bullet}OH + H_2O_2 \xrightarrow{k_2} HO_2^{\bullet} + H_2O$	2.7×10^7 M^{-1} s^{-1}	33
R3	$^{\bullet}OH + HO_2^- \xrightarrow{k_3} HO_2^{\bullet} + OH^-$	7.5×10^9 M^{-1} s^{-1}	34
R4	$HO_2^{\bullet} + H_2O_2 \xrightarrow{k_4} {}^{\bullet}OH + H_2O + O_2$	3 M^{-1} s^{-1}	35
R5	$O_2^{\bullet-} + H_2O_2 \xrightarrow{k_5} {}^{\bullet}OH + O_2 + OH^-$	0.13 M^{-1} s^{-1}	36
R6	$O_2^{\bullet-} + H^+ \xrightarrow{k_6} HO_2^{\bullet}$	1×10^{10} M^{-1} s^{-1}	37
R7	$HO_2^{\bullet} \xrightarrow{k_7} O_2^{\bullet-} + H^+$	1.58×10^5 s^{-1}	37
R8	$^{\bullet}OH + {}^{\bullet}OH \xrightarrow{k_8} H_2O_2$	5.5×10^9 M^{-1} s^{-1}	33
R9	$HO_2^{\bullet} + HO_2^{\bullet} \xrightarrow{k_9} H_2O_2 + O_2$	8.3×10^5 M^{-1} s^{-1}	37
R10	$^{\bullet}OH + HO_2^{\bullet} \xrightarrow{k_{10}} O_2 + H_2O$	6.6×10^9 M^{-1} s^{-1}	38
R11	$HO_2^{\bullet} + O_2^{\bullet-} \xrightarrow{k_{11}} HO_2^- + O_2$	9.7×10^7 M^{-1} s^{-1}	37
R12	$^{\bullet}OH + O_2^{\bullet-} \xrightarrow{k_{12}} O_2 + OH^-$	8×10^9 M^{-1} s^{-1}	39
R13	$H_2O_2 \leftrightarrow H^+ + HO_2^-$	pK_a = 11.6	40
R14	$P_n + {}^{\bullet}OH \xrightarrow{k_{14}} R_n^{\bullet} + H_2O$	to be determined	this study
R15	$R_n^{\bullet} \xrightarrow{k_{15}} \sum_n (R_n^{\bullet} - R_{n-1}^{\bullet}) + R_1^{\bullet}(M_1)$	to be determined	this study
R16	$M_1 + {}^{\bullet}OH \xrightarrow{k_{16}} .... \rightarrow CO_2 + H_2O$	to be determined	this study

limitations, models with an implied number of equations are not easy to solve.

Generally, the polymer degradation is considered as any type of change of a polymer chain involving the main-chain backbone or side groups or both. These changes in an aqueous solution result in the main chain scission and, subsequently, reduce the molecular weights. The main chain scission may take place in one of two ways, or both, which are approximately associated with the reverse of the two types of polymerization processes (condensation and addition polymerization).[41] The scission may occur randomly (random degradation) where chain cleavage occurs at random points along the chain or at the terminal of a polymer radical or polymer where monomer units are successfully released (unzipping). In the former case, which is the reverse of condensation polymerization, the molecular weight decreases continuously with the extent of the reaction. In the latter form of the depolymerization, the monomer production is considerable. This case is the reverse of the propagation step in the vinyl polymerization.

In this study, the chain-end scission (unzipping) is considered as the mechanism of the chain cleavage, since it is usually the case in the complete mineralization.[42] Therefore, the reaction mechanism is based on the degradation of PEO to its monomer (ethylene oxide). The initiation step in the generalized mechanism is the photolysis of H_2O_2 that results in the formation of the highly reactive hydroxyl radicals ($^{\bullet}OH$) that attack the target compound (PEO) and leads to the chain scission. To be more precise, the hydrogen abstraction of the polymer of the chain length n (P_n) results in the generation of the chain-end radical ($R_n^{\bullet}$), as shown in Reaction R14. The β-scission of an end radical leads to the monomer formation (M_1) according to the chain-end scission as presented in Reaction R15. The monomer degradation results in the complete mineralization of the polymer to H_2O and CO_2 (Reaction R16), disregarding the intermediates formed during the course of reactions.

To overcome the difficulties of the kinetic modeling of polymers, models based on population balance equations (PBEs) have been developed.[43−45] PBEs are often applied in fragmentation models to describe how the frequency distribution of different-sized entities, both parent and progeny, evolve. As polymer degradation is a fragmentation phenomenon, continuous-distribution mass (population) balances are applied to study the kinetics of the polymer degradation. A free-radical mechanism is proposed to evaluate rate coefficients based on the continuous-distribution kinetics, which provides the details of the degradation process by taking into account the time dependency of TOC concentration. Broadly, the reaction mechanism often used to describe the degradation of macromolecules comprises three reversible elementary steps: the initiation-termination of radicals, the hydrogen abstraction,[44,46] and the depropagation (scission, decay). As mentioned earlier, the chain-end scission is considered as the main mechanism of the photodegradation. According to the long chain approximation (LCA), initiation-termination steps are neglected because of the insignificant effect on the overall reaction rates.[47,48] As shown in Reaction R14 in Table 3, the hydrogen abstraction by hydroxyl radicals from the polymer of the chain length n results in the formation of radicals of the same chain length ($R_n^{\bullet}$). The binary degradation of $R_n^{\bullet}$ could be represented by the following sequential reactions:

$$R_n^{\bullet} \rightarrow (R_n^{\bullet} - R_{n-1}^{\bullet}) + R_{n-1}^{\bullet}$$
$$R_{n-1}^{\bullet} \rightarrow (R_{n-1}^{\bullet} - R_{n-2}^{\bullet}) + R_{n-2}^{\bullet}$$
$$\vdots$$
$$R_2^{\bullet} \rightarrow (R_2^{\bullet} - R_1^{\bullet}) + R_1^{\bullet}(M_1)$$

which, in turn, could be written as follows:

dx.doi.org/10.1021/ie3005995 | Ind. Eng. Chem. Res. 2012, 51, 14980−14993

$$R_n^{\bullet} \rightarrow (R_n^{\bullet} - R_{n-1}^{\bullet}) + (R_{n-1}^{\bullet} - R_{n-2}^{\bullet}) + ... + (R_2^{\bullet} - R_1^{\bullet}) + R_1^{\bullet}(M_1) \quad (2)$$

Generally, for a binary fragmentation reaction, the product kinetics is represented by eq 3, in which the integral is used instead of the sum to make the calculations easier:[49]

$$R(n) = \int_n^{\infty} k(n')\Omega(n, n')r(n', t)\, dn' \quad (3)$$

where $k(n')$ and $r(n',t)$ are the rate constant of the binary scission and the chain length distribution of the polymer radical, respectively. The stoichiometric coefficient $\Omega(n,n')$ represents the likelihood of obtaining a scission product of the chain length n and $n' - n$ from a larger molecule n'. A general expression for the stoichiometric coefficient, or kernel, is given by the following expression:[49]

$$\Omega(n, n') = \frac{n^m(n' - n)^m\Gamma(2m + 2)}{\Gamma(m + 1)^2(n')^{2m+1}} \quad (4)$$

where Γ is the gamma function and m is a parameter indicating the shape of the scission fragment distribution. For a chain-end scission, when a specific product of a fixed chain length 1 and a chain length of $n' - 1$ are formed, Dirac delta functions are used to represent the stoichiometric kernels, $\Omega(n' - 1,n') = \delta(n - (n' - 1))$ and $\Omega(n,n') = \delta(n - 1)$, respectively.[23] The stoichiometric coefficient $\delta(n - (n' - 1))$ ensures that a product has the chain length of $n = n' - 1$ and that $n' \geq n$ is valid in the interval of the integration. Therefore, based on these assumptions and explanations, a detailed mathematical model was developed in the form of a set of ordinary differential equations (ODEs) representing the kinetic expressions of the principal species in the system. These dynamic model equations that result in a set of stiff ODEs must be solved simultaneously. The model was solved using MATLAB 7.10 (R2010) environment, based on Gear's method. The model predictions were compared to the experimental data carried out under different operating conditions, based on the results of the experimental design.

5. KINETIC PARAMETER ESTIMATION

In order to find the optimal kinetic parameters, the parameter estimation was performed according to the following objective function:[50]

$$\min J(z) = \sum_{i=1}^{N}\left(\frac{TOC_{m,i}(z)}{TOC_i} - 1\right)^2 \quad (5)$$

subject to the obtained dynamic model equations

where

$$z = [k_{14}, k_{15}, k_{16}]^T \quad (6)$$

Here, $J(z)$ is the objective function, $TOC_{m,i}(z)$ and TOC_i are the model prediction and the experimental data for TOC, and N is the number of data points.

The kinetic parameter estimation was carried out for 20 experimental trials with specific operating conditions. Six experimental data points at t = 0, 30, 60, 90, 120, and 150 were used for each of the 20 experimental trials. The MATLAB 7.10 (R2010) optimization toolbox was employed to solve the constrained optimization problem. Solving this problem results in obtaining optimal values of the kinetic parameter z, as defined in eq 6.

The goodness-of-fit between the experimental data and the predicted model was calculated, according to the Theil's inequality coefficient (TIC), as follows:[50]

$$TIC = \frac{\sqrt{\sum_i (TOC_i - TOC_{m,i}(z))^2}}{\sqrt{\sum_i TOC_i^2} + \sqrt{\sum_i TOC_{m,i}^2(z)}} \quad (7)$$

where $TOC_{m,i}(z)$ and TOC_i are the model prediction and the experimental data for TOC, respectively. A TIC value of <0.3 indicates a good agreement between the experimental data and the predicted model values.[50]

6. RESULTS AND DISCUSSION

6.1. Experimental Design. Table 4 depicts the four-factor, five-level CCD and the observed and predicted values for the percent TOC removal by the developed quadratic model. As mentioned earlier, the RSM was used to estimate the parameters indicating an empirical relationship between input variables and the response, as indicated in eq 1. The quadratic model equation for predicting the response function (%TOC removal) was expressed by the following second-order polynomial equation, in terms of the coded factors:

Table 4. Four-Factor, Five-Level CCD for RSM, along with the Observed and Predicted Responses

	Independent Coded Variables				TOC Removal (%)	
run	X_1	X_2	X_3	X_4	observed	predicted
1	−1	−1	−1	−1	66.95	66.94
2	1	−1	−1	−1	60.01	60.7
3	−1	1	−1	−1	69.96	69.99
4	1	1	−1	−1	65.99	63.99
5	−1	−1	1	−1	64.21	61.18
6	1	−1	1	−1	59.48	58.44
7	−1	1	1	−1	68.22	67.82
8	1	1	1	−1	61.68	61.18
9	−1	−1	−1	1	66.29	65.78
10	1	−1	−1	1	61.5	60.62
11	−1	1	−1	1	69.4	69.17
12	1	1	−1	1	66.36	64.25
13	−1	−1	1	1	63.75	64.47
14	1	−1	1	1	59.68	58.67
15	−1	1	1	1	69.01	67.3
16	1	1	1	1	62.99	61.74
17	−2	0	0	0	73.83	73.21
18	2	0	0	0	58.51	61.43
19	0	−2	0	0	53.49	52.79
20	0	2	0	0	55.95	58.91
21	0	0	−2	0	67.95	69.35
22	0	0	2	0	64.34	65.23
23	0	0	0	−2	66.5	66.43
24	0	0	0	2	63.5	65.83
25	0	0	0	0	63.28	63.33
26	0	0	0	0	62.6	63.33
27	0	0	0	0	61.8	63.33
28	0	0	0	0	63.18	63.33
29	0	0	0	0	64.71	63.33
30	0	0	0	0	64.19	63.33
31	0	0	0	0	63.52	63.33

dx.doi.org/10.1021/ie3005995 | Ind. Eng. Chem. Res. 2012, 51, 14980−14993

Table 5. ANOVA for the Prediction of Percent of TOC Removal by the Quadratic Model

	Statistics					
factors (coded)	sum of squares	df[a]	mean square	*F*-value	*p*-value, Prob > *F*	remark
model	481.14	14	34.37	10.85	<0.0001[b]	significant
X_1	208.51	1	208.51	65.84	<0.0001	significant
X_2	56.00	1	56.00	17.68	0.0007	significant
X_3	25.34	1	25.34	8.00	0.0121	significant
X_4	0.52	1	0.52	0.16	0.6917	
X_1X_2	0.058	1	0.058	0.018	0.8944	
X_1X_3	0.43	1	0.43	0.14	0.7176	
X_1X_4	1.13	1	1.13	0.36	0.5579	
X_2X_3	0.30	1	0.30	0.094		
X_1X_4	0.11	1	0.11	0.035	0.8530	
X_3X_4	0.090	1	0.090	0.028	0.8682	
X_1^2	28.36	1	28.36	8.96	0.0086	significant
X_2^2	99.64	1	99.64	31.46	<0.0001	significant
X_3^2	28.00	1	28.00	8.84	0.0090	significant
X_4^2	14.15	1	14.15	4.47	0.0506	
pure error	5.58	6	0.93			
cor total[c]	531.81	30				
R^2 = 0.9047						
adjusted R^2 = 0.8214						
adequate precision = 16.48						

[a]Degree of freedom. [b]A value of $p < 0.05$ is considered to be significant. [c]Corrected total sum of squares.

$$Y = 63.33 - 2.95X_1 + 1.53X_2 - 1.03X_3 - 0.15X_4 + 0.06X_1X_2 - 0.16X_1X_3 + 0.27X_1X_4 - 0.14X_2X_3 + 0.084X_2X_4 + 0.075X_3X_4 + X_1^2 - 1.87X_2^2 + 0.99X_3^2 + 0.70X_4^2 \quad (8)$$

The quadratic model equation can be recalculated considering only the significant factors. The statistical significance of the second-order polynomial model to predict the percent TOC removal was tested by the analysis of variance (ANOVA). The results of the ANOVA are presented in Table 5. The significance of each coefficient in eq 8 was determined by the Fisher's *F*-test and values of probability greater than *F*. As shown in Table 5, a small probability value ($p < 0.0001$) indicates that the model was highly significant. The goodness-of-fit of the model was validated by the determination coefficient (R^2). High R^2 values show the high significance of the model. Also, the adequate precision greater than 4 (16.48 in this case) shows that the model could be used to navigate the design space defined by the CCD. Adequate precision is a measure of the range in the predicted response relative to its associated error (i.e., a signal-to-noise ratio). The normality of the data could be checked through the normal probability plot of the residuals. If the points on the plot lie on a straight line, the residuals are normally distributed, as confirmed in Figure 2. Also, a high correlation between observed and predicted data shown in Figure 3 indicates their low discrepancies.

In order to study the interaction effects between the variables (the initial concentration of polymer, the initial concentration of H_2O_2, pH, and the recirculation rate), the 3D response surface and 2D contour curves based on the quadratic model were plotted, as shown in Figures 4a–f. As illustrated in those figures, the percent TOC removal was significantly affected by the initial concentrations of polymer and H_2O_2. It could be seen that the percent TOC removal decreases by increasing the initial polymer concentration within the experimental range.

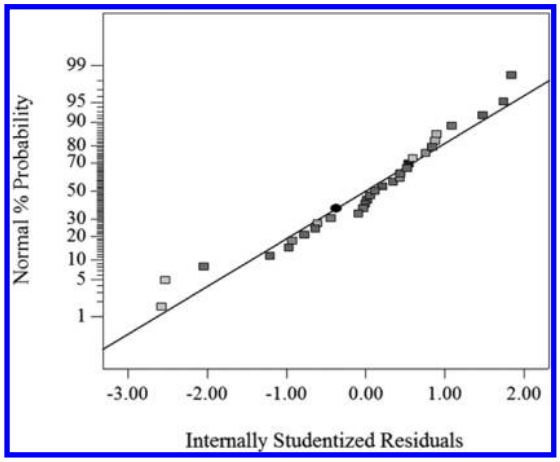

Figure 2. Validation of percent TOC removal model using the normal probability plot of internally studentized residuals.

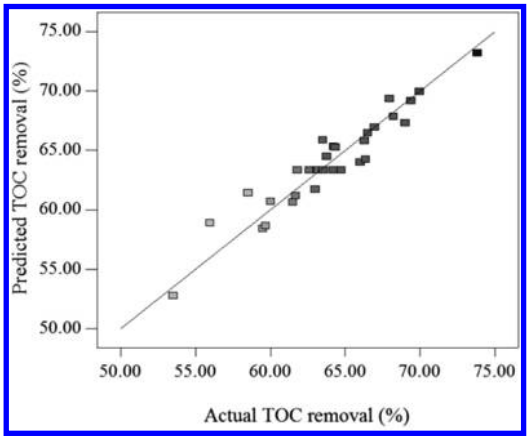

Figure 3. Validation of percent TOC removal model using the plot of predicted values versus observed experimental data.

dx.doi.org/10.1021/ie3005995 | *Ind. Eng. Chem. Res.* 2012, 51, 14980–14993

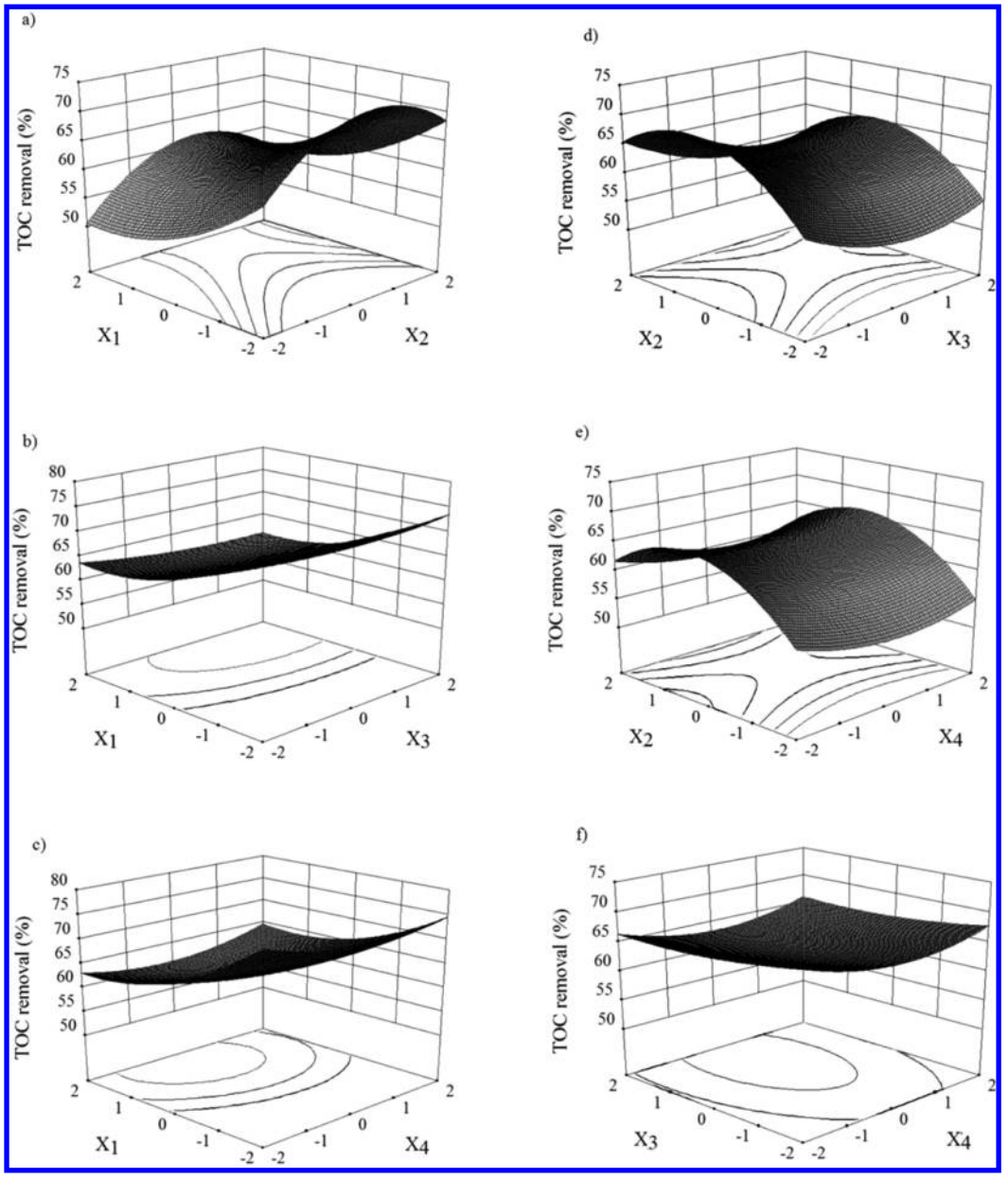

Figure 4. Interaction effects of different parameters on the percent TOC removal using 3D response surface and 2D contours: (a) polymer concentration and H_2O_2 concentration, (b) polymer concentration and pH, (c) polymer concentration and recirculation rate, (d) H_2O_2 concentration and pH, (e) H_2O_2 concentration and recirculation rate, and (f) pH and recirculation rate.

The effect of the initial concentration of PEO on the percent TOC removal is mainly due to the absorption of UV radiation by PEO molecules. An increase in the initial concentration of PEO leads to induce an inner filter effect.[51] Therefore, the permeability of the UV light becomes less at higher concentration of PEO, as it can be also verified later by eq 14 that higher concentration of PEO results in higher UV absorption by PEO.[51] This results in decreasing the UV radiation absorption by H_2O_2 and subsequently less formation of hydroxyl radicals, which are the major cause of the PEO decomposition. Increasing the initial concentration of H_2O_2 results in enhancing the percent TOC removal up to an optimum concentration of H_2O_2, where the trend reverses after this point. This is due to the fact that the excess H_2O_2 scavenges hydroxyl radicals.[52,53] Also, it can be seen that the percent TOC removal decreases at higher pH where the maximum percent TOC removal is achieved at the lower initial pH. In alkaline solutions, the dissociated form of hydrogen peroxide (HO_2^-) reacts with hydroxyl radicals more than 2 orders of magnitude faster than hydrogen peroxide (Reactions R2 and R3). Therefore, the oxidation efficiency decreases as hydroxyl radicals are consumed. However, as is evident in Figures 4a–f, the influence of the pH on the percent TOC removal is less pronounced than the initial polymer concentration and initial H_2O_2 dosage. Also, as shown in Table 5 and Figures 4c, 4e, and 4f, the recirculation rate does not have any significant effect on the percent TOC removal. This is also confirmed in Table 5, which shows the significance of the factors and their interaction.

6.2. Optimization of Operating Conditions. The RSM was used to determine the values of the four independent variables that result in a maximum percent TOC removal. The optimization of experimental conditions was carried out by maximizing the percent TOC removal at defined optimization

dx.doi.org/10.1021/ie3005995 | Ind. Eng. Chem. Res. 2012, 51, 14980–14993

criteria for the factors. Therefore, the optimum operating conditions were found using the numerical technique built into the Design Expert Software 8.0.5, according to the predicted model. The numerical optimization searches the design space using the developed model in the analysis to find factor settings that meet the goal of maximizing TOC removal. The optimum values to achieve the maximum TOC removal of 84% after 150 min were 10 mg L^{-1} PEO, 780 mg L^{-1} H_2O_2, pH 3, and a recirculation rate of 0.5 L min^{-1}. The TOC removal efficiency was tested experimentally under the optimum operating conditions to validate the model prediction. Eighty two percent (82%) TOC removal was achieved under the optimal operating conditions, which confirmed the results of the developed model.

6.3. Kinetic Model Development and Reactor Modeling. A mathematical model was developed in the form of a set of ODEs that were based on the reaction scheme presented in Table 3. The proposed model represents the kinetic expressions of the principal species in the system. The primary reaction that initiates the chain reaction is the direct photolysis of H_2O_2 to two hydroxyl radical molecules, as shown below:

$$R_{UV,H_2O_2} = \varphi_{H_2O_2} e_\lambda^a \tag{9}$$

where $\varphi_{H_2O_2}$ is the quantum yield of H_2O_2 and HO_2^- (expressed in units of mol $Einstein^{-1}$) and e_λ^a is the local volumetric rate of energy absorption (LVREA) (given in units of Einstein L^{-1} s^{-1}).

H_2O_2 and HO_2^-, which are acid−base conjugates, are interrelated through the equilibrium reaction described by Reaction (R13). The total concentration of H_2O_2 at equilibrium is defined as follows:[22]

$$[H_2O_2]_T = [H_2O_2] + [HO_2^-] \tag{10}$$

Consequently, a new equilibrium concentration for the two individual species can be expressed as follows:[9,22]

$$[H_2O_2] = \frac{[H_2O_2]_T}{1 + K_a[H^+]^{-1}} \tag{11}$$

$$[HO_2^-] = \frac{[H_2O_2]_T}{1 + K_a^{-1}[H^+]} \tag{12}$$

where K_a is the equilibrium constant. These concentrations are used later in the developed kinetic model. The LVREA, based on the radiation balance, is defined according to the Beer−Lambert law as follows:[22]

$$e_\lambda^a = I_o\left(\frac{\varepsilon_{H_2O_2}[H_2O_2] + \varepsilon_{HO_2^-}[HO_2^-]}{\varepsilon_{H_2O_2}[H_2O_2] + \varepsilon_{HO_2^-}[HO_2^-] + \varepsilon_{TOC_1}[TOC_1]}\right) \times \left(1 - \exp\left\{-2.303b\left(\varepsilon_{H_2O_2}[H_2O_2] + \varepsilon_{HO_2^-}[HO_2^-] + \varepsilon_{TOC_1}[TOC_1]\right)\right\}\right) \tag{13}$$

where I_o, the intensity of the incident light, was calculated to be 1.97×10^{-5} Einstein L^{-1} s^{-1}, which is the light incident at 254-nm photon irradiance estimated from the 14 W LP lamp over the photoreactor volume, assuming 10% attenuation by the quartz sleeve and 33% efficiency for the LP lamp. $[TOC_1]$ is the molar TOC concentration of PEO. The fraction shows the portion of the UV radiation absorption by hydrogen peroxide. Parameters $\varepsilon_{H_2O_2}$, $\varepsilon_{HO_2^-}$, and ε_{TOC_1} are the molar extinction coefficients of H_2O_2 (18.7 M^{-1} cm^{-1}),[21] HO_2^- (210 M^{-1} cm^{-1}),[21] and TOC_1 (213.96 M^{-1} cm^{-1}) at 254 nm, and b is the effective path length (annular space) in the photoreactor. The parameter ε_{TOC_1} was determined by measuring the absorbance of several dilutions of the PEO in distilled water by means of a spectrophotometer. The absorbance at 254 nm (A_{254}) is then related to the extinction coefficient (ε) as follows:

$$A_{254} = \varepsilon_{TOC_1} c_{TOC_1} l \tag{14}$$

where c_{TOC_1} and l are the TOC concentration of PEO and the effective path length of the UV radiation in the spectrophotometer (1 cm), respectively. Therefore, the kinetic expressions are obtained by incorporating the decomposition and the production of the species through free-radical reactions as follows:

$$R_{H_2O_2} = (-R_{UV,H_2O_2} - k_2[^\bullet OH][H_2O_2] - k_3[^\bullet OH][HO_2^-] - k_4[HO_2^\bullet][H_2O_2] - k_5[O_2^{\bullet-}][H_2O_2] + k_8[^\bullet OH]^2 + k_9[HO_2^\bullet]^2 + k_{11}[HO_2^\bullet][O_2^{\bullet-}]) \times \left(\frac{1}{1 + K_a[H^+]^{-1}}\right) \tag{15}$$

$$R_{HO_2^-} = (-R_{UV,H_2O_2} - k_2[^\bullet OH][H_2O_2] - k_3[^\bullet OH][HO_2^-] - k_4[HO_2^\bullet][H_2O_2] - k_5[O_2^{\bullet-}][H_2O_2] + k_8[^\bullet OH]^2 + k_9[HO_2^\bullet]^2 + k_{11}[HO_2^\bullet][O_2^{\bullet-}]) \times \left(\frac{1}{1 + K_a^{-1}[H^+]}\right) \tag{16}$$

$$R_{^\bullet OH} = 2R_{UV,H_2O_2} - k_2[^\bullet OH][H_2O_2] - k_3[^\bullet OH][HO_2^-] + k_4[HO_2^\bullet][H_2O_2] + k_5[O_2^{\bullet-}][H_2O_2] - k_8[^\bullet OH]^2 - k_{10}[^\bullet OH][HO_2^\bullet] - k_{12}[^\bullet OH][O_2^{\bullet-}] - k_{14}[P][^\bullet OH] - k_{16}[M][^\bullet OH] \tag{17}$$

$$R_{HO_2^\bullet} = k_2[^\bullet OH][H_2O_2] + k_3[^\bullet OH][HO_2^-] - k_4[HO_2^\bullet][H_2O_2] + k_6[O_2^{\bullet-}][H^+] - k_7[HO_2^\bullet] - k_9[HO_2^\bullet]^2 - k_{10}[^\bullet OH][HO_2^\bullet] - k_{11}[HO_2^\bullet][O_2^{\bullet-}] \tag{18}$$

$$R_{O_2^{\bullet-}} = -k_5[O_2^{\bullet-}][H_2O_2] - k_6[O_2^{\bullet-}][H^+] + k_7[HO_2^\bullet] - k_{11}[HO_2^\bullet][O_2^{\bullet-}] - k_{12}[^\bullet OH][O_2^{\bullet-}] \tag{19}$$

Also, the reaction rates of the polymer, the polymer radical, and the monomer could be written by the following equations:

$$R_p(n, t) = -k_{14}(n)[^\bullet OH]p(n, t) \tag{20}$$

$$R_r(n, t) = k_{14}(n)[^\bullet OH]p(n, t) - k_{15}(n)r(n, t) + \int_n^\infty k_{15}(n')r(n', t)\delta(n - (n' - 1))\, dn' \tag{21}$$

$$R_m(n, t) = \int_n^\infty k_{15}(n')r(n', t)\Omega(1, n')\, dn' - k_{16}(n)[^\bullet OH]m(n, t) \tag{22}$$

dx.doi.org/10.1021/ie3005995 | Ind. Eng. Chem. Res. 2012, 51, 14980−14993

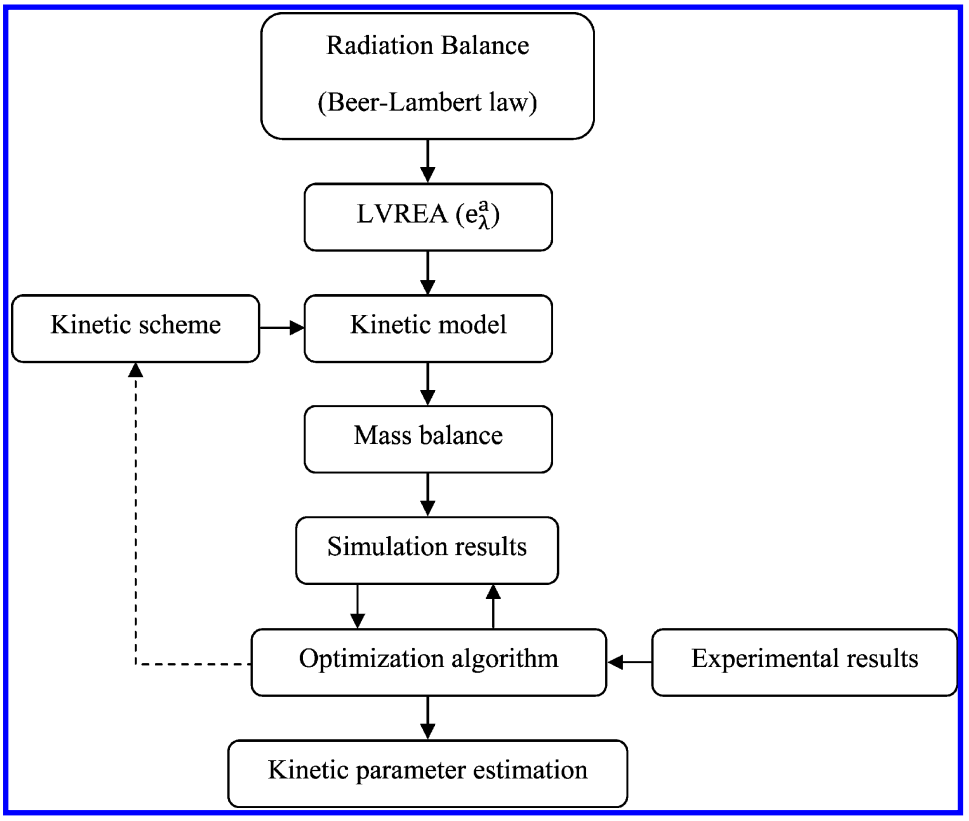

Figure 5. Algorithm of mathematical modeling and computational simulation procedure for kinetic parameter estimation.

In these equations, $p(n,t)$, $r(n,t)$, and $m(n,t)$ represent the chain length distribution of the polymer, the chain end radical, and the monomer, respectively. At small reaction times, all rate coefficients are usually assumed to be independent of the chain length and they could be considered constant.[54,55] In order to make the above equations easy to solve, moment operation is used as follows:

$$r^{(p)}(t) = \int_0^\infty r(n,\, t)n^p \, \mathrm{d}n \tag{23}$$

The zero moment ($p = 0$) is the time-dependent molar concentration of the polymer and the first moment ($p = 1$) is the mass concentration. Therefore, applying moment operation results in the following equations:[56,57]

$$\mathrm{R}_{p^{(p)}} = -k_{14}[^\bullet\mathrm{OH}]p^{(p)} \tag{24}$$

$$\mathrm{R}_{r^{(p)}} = k_{14}[^\bullet\mathrm{OH}]p^{(p)} - k_{15}r^{(p)} + k_{15}\sum_{j=0}^{k}(-1)^j r^{(k-j)} \tag{25}$$

$$\mathrm{R}_{m^{(p)}} = k_{15}r^{(0)} - k_{16}[^\bullet\mathrm{OH}]m^{(p)} \tag{26}$$

As mentioned previously, the zero moment represents the molar ccentration of the polymer, where the TOC concentration is considered as the output parameter. Therefore, the zero moment was applied to eqs 24−26 and $[\mathrm{TOC}_1]$ and $[\mathrm{TOC}_2]$ concentrations were considered as the molar TOC concentrations of polymer and monomer as follows:

$$\mathrm{R}_{\mathrm{TOC}_1} = -k_{14}[^\bullet\mathrm{OH}][\mathrm{TOC}_1] \tag{27}$$

$$\mathrm{R}_{r^{(0)}} = k_{14}[^\bullet\mathrm{OH}][\mathrm{TOC}_1] \tag{28}$$

$$\mathrm{R}_{\mathrm{TOC}_2} = k_{15}r^{(0)} - k_{16}[^\bullet\mathrm{OH}][\mathrm{TOC}_2] \tag{29}$$

Therefore, eq 17 must be modified as follows:

$$\begin{aligned}\mathrm{R}_{^\bullet\mathrm{OH}} = {} & 2\mathrm{R}_{\mathrm{UV,H_2O_2}} - k_2[^\bullet\mathrm{OH}][\mathrm{H_2O_2}] - k_3[^\bullet\mathrm{OH}][\mathrm{HO_2^-}] \\ & + k_4[\mathrm{HO_2^\bullet}][\mathrm{H_2O_2}] + k_5[\mathrm{O_2^{\bullet -}}][\mathrm{H_2O_2}] - k_8[^\bullet\mathrm{OH}]^2 \\ & - k_{10}[^\bullet\mathrm{OH}][\mathrm{HO_2^\bullet}] - k_{12}[^\bullet\mathrm{OH}][\mathrm{O_2^{\bullet -}}] - k_{14}[\mathrm{TOC}_1] \\ & [^\bullet\mathrm{OH}] - k_{16}[\mathrm{TOC}_2][^\bullet\mathrm{OH}]\end{aligned} \tag{30}$$

The general mass balance equation given by eq 31 is used to interpret the experimental data in the batch recirculation system:[58]

$$\frac{\partial C_i}{\partial t} + \nabla \cdot N_i = R_i \tag{31}$$

where C_i is the molar concentration of component i in the reacting system, t the time, N_i the molar flux of component i, and R_i the homogeneous molar reaction rate of the component i. The general mass balance equation must be applied to the recirculating batch photoreactor. If the system works under the well-stirred conditions (the ratio of the photoreactor volume to the total volume ($V_\mathrm{P}/V_\mathrm{T} \ll 1$, 0.092 in this case) and high recirculating flow rate to ensure small conversion per pass (<5%), the rate of change of the concentration in the tank could be written as follows:[59]

$$\frac{\mathrm{d}C_i}{\mathrm{d}t} = \frac{V_\mathrm{R}}{V_\mathrm{T}}(\mathrm{R}_i) \tag{32}$$

Therefore, the dynamic model eqs 15, 16, 18, and 19, along with eqs 27−30, are substituted into eq 32 for each species and the obtained set of stiff ODES are solved simultaneously. The

dx.doi.org/10.1021/ie3005995 | Ind. Eng. Chem. Res. 2012, 51, 14980−14993

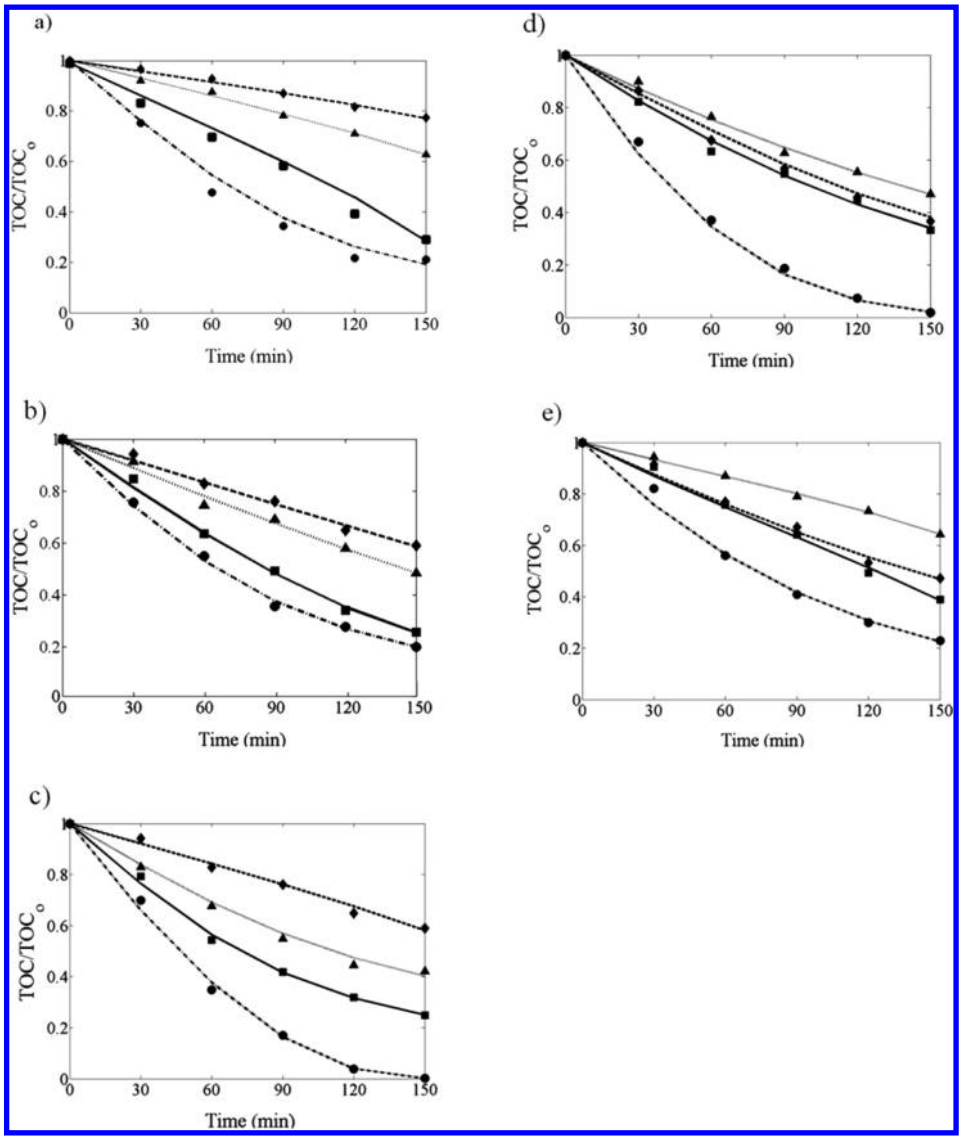

Figure 6. Comparison of model predictions and experimental data of TOC/TOC$_o$ as a function of time for different initial concentration of H_2O_2 [mg L^{-1}]: (a) 300, (b) 500, (c) 700, (d) 900, and (e) 1100 (PEO$_o$ [mg L^{-1}]: (●) 10, (■) 20, (▲) 30, and (◆) 50). The lines are the corresponding model predictions. Initial conditions: T = 22 °C, natural pH, and recirculation rate = 2 L min^{-1}.

model was solved using the MATLAB 7.10 (R2010) environment, based on Gear's method. The numerical algorithm is a variable-order solver based on the numerical differentiation formulas. The proposed model needs to be validated, as shown in the next section. The algorithm used for simulation and the kinetic parameter estimation is illustrated in Figure 5.

6.4. Model Validation and Kinetic Parameter Estimation. In order to validate the proposed model, the model predictions are compared to the experimental data carried out under different operating conditions, based on the results of the experimental design. The most influential factors were found to be initial concentrations of PEO and H_2O_2, as illustrated in Table 5. The pH was not controlled during the experiments, since its effect was less pronounced, in comparison to other factors. Therefore, a set of experiments were carried out at different initial concentrations of PEO (10, 20, 30, and 50 mg L^{-1}) and initial concentrations H_2O_2 (300, 500, 700, 900, and 1,100 mg L^{-1}). The recirculation rate was kept constant at 2 L min^{-1}, and the pH was at the natural pH of the solution (5.5 ± 0.5). Therefore, the experimentally determined values of the normalized TOC are compared with the model predictions in Figures 6a–e. Since there was no pH adjustment during these experiments, there are some discrepancies between these results of model validation and some of the experimental design runs in the first part of the study. As illustrated in Figures 6a–e, the proposed model provided accurate predictions of the percent TOC removal, as a function of reaction time, suggesting that no major contributor to the overall kinetic model was ignored. The calculated TICs < 0.3 (Table 6) for all experimentally tested conditions indicate that there is an excellent agreement between the model predictions and the experimental data. Also, Figures 6a–e show that as the initial concentration of PEO increases (for all initial concentrations of H_2O_2), the percent TOC removal decreases. As mentioned previously, higher UV radiation absorption by PEO results in less UV penetration to the solution. Therefore, less UV radiation is available for H_2O_2 to generate oxidant radicals.

The initial H_2O_2 concentration is also a significant parameter in the UV/H_2O_2 process. The effect of the initial concentration of H_2O_2 on the percent TOC removal of PEO was also studied

dx.doi.org/10.1021/ie3005995 | Ind. Eng. Chem. Res. 2012, 51, 14980–14993

Table 6. Optimization and Simulation Results for the Kinetic Rate Constants

H_2O_2 dosage (mg L^{-1})	PEO concentration (mg L^{-1})	Rate Constants $k_{14} \times 10^{-8}$ (M^{-1} s^{-1})	Rate Constants $k_{15} \times 10^{-2}$ (s^{-1})	Rate Constants $k_{16} \times 10^{-6}$ (M^{-1} s^{-1})	TIC
300	10	24.61	10.79	2.04	0.0434
	20	15.34	6.5	3.51	0.0177
	30	5.58	8.3	1.79	0.0053
	50	4.16	7.6	1.53	0.0254
500	10	12.16	6.25	4.25	0.0135
	20	18.79	13.18	1.97	0.0123
	30	8.06	0.13	1.76	0.0099
	50	6.35	2.36	1.56	0.0369
700	10	23.93	52.5	46.58	0.0326
	20	24.58	14.01	32.29	0.0157
	30	16.94	11.89	5.68	0.0338
	50	20.5	15.69	1.76	0.0105
900	10	22.32	35.1	38.41	0.0668
	20	25.57	2.88	4.57	0.0172
	30	4.16	1.25	8.99	0.0118
	50	6.01	19.9	3.76	0.0145
1100	10	6.1	10.72	10.43	0.0288
	20	3.15	28.6	1.44	0.0148
	30	1.47	4.12	5.46	0.0048
	50	6.96	1.22	8.48	0.0163

by varying the initial concentration of H_2O_2 from 300 mg L^{-1} to 1100 mg L^{-1} for the initial concentrations of PEO from 10 mg L^{-1} to 50 mg L^{-1}, as shown in Figures 4 and 6. As is evident, there is an optimum value for the initial concentration of H_2O_2 above which the percent TOC removal decreases. For initial concentrations of PEO of 10, 20, and 30 mg L^{-1}, the optimum initial dosage of H_2O_2 was found to be 700 mg L^{-1}, but for the initial concentration of 50 mg L^{-1} PEO, the optimum initial concentration of H_2O_2 was 900 mg L^{-1}, as illustrated in Figure 7. This finding indicates that, as the initial concentration of PEO increases, more H_2O_2 is needed to achieve a maximum percent TOC removal. An excess amount of H_2O_2 acts as a scavenger of hydroxyl radicals (Reaction R2), which forms hydroperoxyl radicals ($HO_2^{\bullet}$) with less reactivity than hydroxyl radicals. Also, the excess amount of hydroperoxyl radical itself acts as a scavenger of hydroxyl radicals, as shown in Reaction R10 and subsequently reduces the degradation rate. Some findings in Table 4 have discrepancies with those of Figure 6, since the pH was not adjusted during the second set of experiments shown in Figure 6.

Apart from these apparent experimental conclusions, one of the main objectives of this study was to achieve the kinetic parameters that best fit the percent TOC removal based on the developed mathematical model under different operating conditions. The validated model could be used to determine rate constants, providing the necessary information for scaling-up purposes. The optimal kinetic parameters were found by solving the objective function (eq 5), subjected to the kinetic model eqs 15, 16, 18, 19, and 27−30. The results are presented in Table 6. The optimization algorithm gives the values of the parameters that minimize the sum of squares of the errors between model predictions and the experimental data. The initial guesses of the rate constants were selected according to the range of acceptable values reported in the open literature.[33] It must be noted that obtained optimal values, that are in acceptable range, are not assumed to be the global ones, because they are highly dependent on the initial guesses. Similar to the most of optimization problems, there is no test showing that the achieved optimal values are the global ones. However, the estimated optimal values are independent of the photoreactor configuration; therefore, they could be used as the starting point for designing commercial-scale photoreactors.

7. CONCLUSIONS

The response surface methodology (RSM) using four-factor, five-level central composite design (CCD) and quadratic programming showed reliable results for the photodegradation of polyethylene oxide (PEO) by the UV/H_2O_2 process. Predicted results from the response functions were in good agreement with the experimental data, confirming the reliability of the employed methodology. Furthermore, results indicated that the initial concentration of PEO, the initial concentration of H_2O_2, and pH had considerable influence on the total organic carbon (TOC) removal efficiency. The recirculation rate had no effect on the response function. From an analysis of the contour plots, it was observed that a decrease in the initial concentration of PEO, an increase in the initial concentration

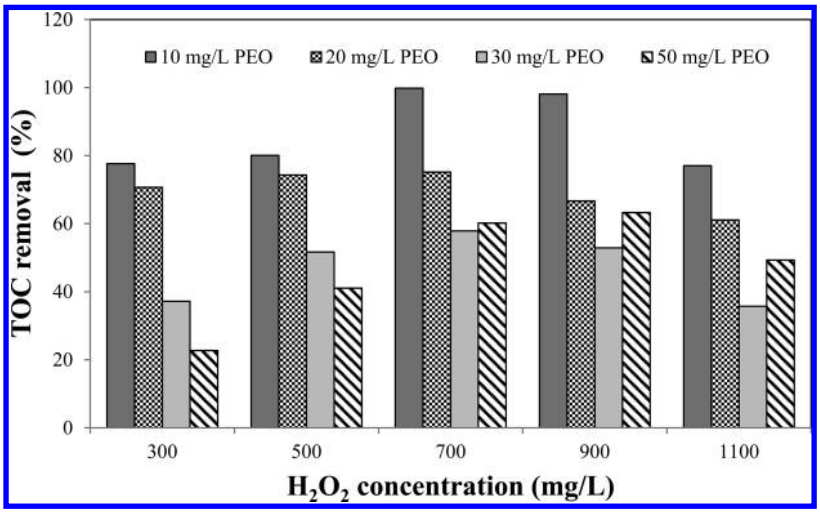

Figure 7. Effect of the initial concentration of H_2O_2 on percent TOC removal at various initial concentrations of PEO.

of H_2O_2 (up to a certain level), and an acidic pH condition result in an increase in the percent TOC removal. The optimum percent TOC removal (84%) was found after 150 min under the operating conditions of 10 mg L^{-1} PEO, 780 mg L^{-1} H_2O_2, pH 3, and a recirculation rate of 0.5 L min^{-1}, based on the developed quadratic model. A mathematical model was developed based on the mass balance of the main species present in water to predict the percent TOC removal of PEO. The continuous distribution was used to establish the kinetic modeling of PEO based on the TOC as a surrogate parameter. Different initial concentrations of PEO and H_2O_2, which were the most influential factors in the percent TOC removal, were used to validate the model. An excellent agreement between the model predictions and the experimental data was confirmed by calculating the Theil's inequality coefficient (TIC) for each experimentally tested parameter. The kinetic parameters were estimated using an optimization algorithm. The obtained kinetic parameters were found to be in the acceptable range of reported values in the open literature. However, they are not assumed to be the global ones. Therefore, the proposed model explaining the free-radical-induced degradation of PEO by the UV/H_2O_2 process could be characterized as an accurate and interpretable model that could be used as a base for the future studies, with the goal of process optimization.

AUTHOR INFORMATION

Corresponding Author

*Tel.: +1 416 9795000, Ext. 6555. Fax: +1 416 9795083. E-mail: mmehrvar@ryerson.ca.

Notes

The authors declare no competing financial interest.

ACKNOWLEDGMENTS

The financial support of the Natural Sciences and Engineering Research Council of Canada (NSERC) and Ryerson University is gratefully appreciated.

NOMENCLATURE

X_1 = initial PEO concentration [mg L^{-1}]
A_{254} = UV absorbance at 254 nm
b = UV path length in the photoreactor [cm]
X_2 = initial H_2O_2 dosage [mg L^{-1}]
X_3 = pH
C_i = concentration of chemical species in water [M]
c_{TOC_1} = TOC concentration of PEO [M]
X_4 = recirculation flow rate [L min^{-1}]
e = residuals
e^a_λ = local volumetric rate of energy absorption [Einstein L s^{-1}]
I_o = UV light intensity [Einstein L^{-1} s^{-1}]
$J_{(z)}$ = objective function
k = rate constant [M^{-1} s^{-1} or s^{-1}]
K_a = equilibrium constant
l = UV path length in the spectrophotometer [cm]
m = parameter indicating the shape of the scission fragment distribution
$m(n,t)$ = chain length distribution of monomer
n = chain length
N_i = molar flux [mol cm^{-2} s^{-1}]
$p(n,t)$ = chain length distribution of polymer
P_n = polymer of chain length n
$r^{(p)}$ = pth order moment operation
$r(n,t)$ = chain length distribution of end radical
R_i = reaction rate [M^{-1} s^{-1}]
$R^\bullet_n$ = polymer radical of chain length n
t = time [s or min]
V_i = volume [L]
x_i, x_j = independent variables
Y = predicted TOC response [%]
z = optimal values of the kinetic parameter

Greek Letters

β_0 = constant coefficient (intercept)
β_i = linear coefficient
β_{ii} = quadratic coefficient
β_{ij} = interaction coefficient
Γ = gamma function
Ω = kernel function
δ = Dirac delta function
ε = molar extinction coefficient [M^{-1} cm^{-1}]
λ = wavelength [nm]
φ = quantum yield [mol $Einstein^{-1}$]

Acronyms

ANOVA = analysis of variance
AOTs = advanced oxidation technologies
CCD = central composite design
df = degrees of freedom
F-value = Fisher's value
LCA = long chain approximation
LVREA = local volumetric rate of energy absorption
M = monomer
ODEs = ordinary differential equations
p-value = probability value
PBEs = population balance equations
PEO = polyethylene oxide
RSM = response surface methodology
TIC = Theil's inequality coefficient
TOC = total organic carbon
UV = ultraviolet

REFERENCES

(1) Bénard, A. C.; Darcos, V.; Drakides, C.; Casellas, C.; Coudane, J.; Vert, M. Fluorescence verses radioactivity labeling for lab-scale investigation of the fate of water-soluble polymers in wastewater treatment plants. *J. Polym. Environ.* **2011**, *19*, 40.

(2) Williams, P. A. In *Handbook of Industrial Water Soluble Polymers*; Williams, P. A., Ed.; Blackwell Publishing, Inc.: Ames, IA, 2007; Chapter 1.

(3) Hassouna, F.; Mailhot, G.; Morlat-Thérias, S.; Gardette, J. L. Influence of iron salts on the photooxidation of poly(*N*-vinyl-pyrrolidone) in aqueous solution. *J. Photochem. Photobiol. A* **2011**, *218*, 239.

(4) Swift, G. Directions for environmentally bioderadable polymer research. *Acc. Chem. Res.* **1993**, *26*, 105.

(5) Giroto, J. A.; Teixeira, A. C. S. C.; Nascimento, C. A. O.; Guardani, R. Degradation of Poly(ethylene glycol) in aqueous solution by photo-Fenton and H_2O_2/UV processes. *Ind. Eng. Chem. Res.* **2010**, *49*, 3200.

(6) Aarthi, T.; Shaama, M. S.; Madras, G. Degradation of water soluble polymers under combined ultrasonic and ultraviolet radiation. *Ind. Eng. Chem. Res.* **2007**, *46*, 6204.

(7) Aidan, A.; Mehrvar, M.; Ibrahim, T. H.; Nenov, V. Particulates and bacteria removal by ceramic microfiltration, UV photolysis, and their combination. *J. Environ. Sci. Health, Part A* **2007**, *42*, 895.

(8) Barrera, M.; Mehrvar, M.; Gilbride, K. A.; McCarthy, L. H.; Laursen, A. E.; Bostan, E.; Pushchak, R. Photolytic treatment of organic constituents and bacterial pathogens in secondary effluent of

synthetic slaughterhouse wastewater. *Chem. Eng. Res. Des.* **2012**, *90*, 1335.
(9) Edalatmanesh, M.; Dhib, R.; Mehrvar, M. Kinetic modeling of aqueous phenol degradation by UV/H_2O_2 process. *Int. J. Chem. Kinet.* **2008b**, *40*, 34.
(10) Poyatos, J. M.; Monio, M. M.; Almecija, M. C.; Torres, J. C.; Hontoria, E.; Osorio, F. Advanced oxidation processes for wastewater treatment: state of the art. *Water Air Soil Pollut.* **2010**, *205*, 187.
(11) Cao, W.; Mehrvar, M. Slaughterhouse wastewater treatment by combined anaerobic baffled reactor (ABR) and UV/H_2O_2 processes. *Chem. Eng. Res. Des.* **2011**, *89*, 1136.
(12) Mohajerani, M.; Mehrvar, M.; Ein-Mozaffari, F. An overview of the integration of advanced oxidation technologies and other processes for water and wastewater treatment. *Int. J. Eng.* **2009**, *3*, 120.
(13) Mohajerani, M.; Mehrvar, M.; Ein-Mozaffari, F. Photoreactor design and CFD modelling of a UV/H_2O_2 process for distillery wastewater treatment. *Can. J. Chem. Eng.* **2012**, *90*, 719.
(14) Oppenländer, T. *Photochemical Purification of Water and Air: Advanced Oxidation Processes*; Wiley−VCH: Weinheim, Germany, 2003; Chapter 6.
(15) Glaze, W. H.; Kang, J. W.; Chapin, D. H. The chemistry of water treatment processes involving ozone, hydrogen peroxide and ultraviolet radiation. *Ozone Sci. Eng.* **1987**, *9*, 335.
(16) Adams, C. D.; Kuzhikannil, J. J. Effects of UV/H_2O_2 preoxidation on the aerobic biodegradability of quaternary amine surfactants. *Water Res.* **2000**, *34*, 668.
(17) Tabrizi, G. B.; Mehrvar, M. Integration of advanced oxidation technologies and biological processes: Recent developments, trends, and advances. *J. Environ. Sci. Health., Part A* **2004**, *39*, 3029.
(18) Tabrizi, G. B.; Mehrvar, M. Pilot-plant study for the photochemical treatment of aqueous linear alkylbenzene sulfonate. *Sep. Purif. Technol.* **2006**, *49*, 115.
(19) Johnson, M. B.; Mehrvar, M. Aqueous metronidazole degradation by UV/H_2O_2 process in single-and multi-lamp tubular photoreactors: Kinetics and reactor design. *Ind. Eng. Chem. Res.* **2008**, *47*, 6525.
(20) Mohajerani, M.; Mehrvar, M.; Ein-Mozaffari, F. CFD modeling of metronidazole degradation in water by UV/H_2O_2 process in single and multi-lamp photoreactors. *Ind. Eng. Chem. Res.* **2010**, *49*, 5347.
(21) Tarr, M. A. *Chemical Degradation Methods for Wastes and Pollutants*; Marcel Dekker: New York, 2003; Chapter 1.
(22) Ghafoori, S.; Mehrvar, M.; Chan, P. Kinetic study of photodegradation of water soluble polymers. *Iran. Polym. J.* **2012**, DOI: 10.1007/s13726-012-0091-5.
(23) Konaganti, V. K.; Madras, G. Photooxidative and pyrolytic degradation of methyl methacrylate−alkyl acrylate copolymers. *Polym. Degrad. Stab.* **2009**, *94*, 1325.
(24) Huang, J.; Yang, J.; Chyu, M. K.; Wang, Q.; Zhu, Z. Continuous-distribution kinetics for degradation of polybutylene terephtalate (PBT) in supercritical methanol. *Polym. Degrad. Stab.* **2009**, *94*, 2142.
(25) Ocampo-Pérez, R.; Sánchez-Polo, M.; Rivera-Utrilla, J.; Leyva-Ramos, R. Degradation of antineoplastic cytarabine in aqueous phase by advanced oxidation processes based on ultraviolet radiation. *Chem. Eng. J.* **2010**, *165*, 581.
(26) Beltrán, F. J.; Aguinaco, A.; García-Araya, J. F. Kinetic modeling of TOC removal in the photocatalytic ozonation of diclofenac aqueous solutions. *Appl. Catal., B* **2011**, *100*, 289.
(27) Marugán, J.; van Grieken, R.; Pablos, C.; Satuf, M. L.; Cassano, A. E.; Alfano, O. M. Rigorous kinetic modelling with explicit radiation absorption effects of the photocatalytic inactivation of bacteria in water using suspended titanium dioxide. *Appl. Catal., B* **2011**, *102*, 404.
(28) Ay, F.; Catalkaya, E. C.; Kargi, F. A statistical experiment design approach for advanced oxidation of Direct Red azo-dye by photo-Fenton treatment. *J. Hazard. Mater.* **2009**, *162*, 230.
(29) Tanyildizi, M. S. Modeling of adsorption isotherms and kinetics of reactive dye from aqueous solution by peanut hull. *Chem. Eng. J.* **2011**, *168*, 1234.
(30) Hasan, S. H.; Srivastava, P.; Talat, M. Biosorption of lead using immobilized Aeromonas hydrophila biomass in up flow column system: Factorial design for process optimization. *J. Hazard. Mater.* **2010**, *177*, 312.
(31) Crittenden, J. C.; Hu, S.; Hand, D. W.; Green, S. A. A kinetic model for H_2O_2/UV process in a completely mixed batch reactor. *Water Res.* **1999**, *33*, 2315.
(32) Giroto, J. A.; Teixeira, A. C. S. C.; Nascimento, C. A. O.; Guardani, R. Degradation of poly(ethylene glycol) in aqueous solution by photo-Fenton and H_2O_2/UV processes. *Ind. Eng. Chem. Res.* **2010**, *49*, 3200.
(33) Buxton, G. V.; Greenstock, C. L.; Helman, W. P.; Ross, A. B. Critical review of rate constants for reactions of hydrated electrons, hydrogen atoms and hydroxyl radicals ($^{\bullet}OH/^{\bullet}O^{-}$) in aqueous solution. *J. Phys. Chem. Ref. Data.* **1988**, *17*, 513.
(34) Christensen, H.; Sehested, K.; Corfitzen, H. Reactions of hydroxyl radicals with hydrogen peroxide at ambient and elevated temperatures. *J. Phys. Chem.* **1982**, *86*, 1588.
(35) Koppenol, W. H.; Butler, J.; Van Leeuwen, J. W. The Haber−Weiss cycle. *Photochem. Photobiol.* **1978**, *28*, 655.
(36) Weinstein, J.; Bielski, B. H. J. Kinetics of the interaction of HO_2 and O_2^- radicals with hydrogen peroxide: The Haber−Weiss reaction. *J. Am. Chem. Soc.* **1979**, *101*, 58.
(37) Bielski, B. H. J.; Cabelli, D. E.; Arudi, R. L.; Ross, A. B. Reactivity of HO_2/O_2^- radicals in aqueous solution. *J. Phys. Chem. Ref. Data* **1985**, *14*, 1041.
(38) Elliot, A. J.; Buxton, G. V. Temperature dependence of the reactions OH + O_2^- and OH + HO_2 in water up to 200°C. *J. Chem. Soc., Faraday Trans.* **1992**, *88*, 2465.
(39) Linden, K. G.; Sharpless, C. M.; Andrews, S.; Atasi, K.; Korategere, V.; Stefan, M.; Suffet, I. H. M. *Innovative UV Technologies to Oxidize Organic and Organoleptic Chemicals*; IWA Publishing: London, 2005; Chapter 8.
(40) Perry, R. H.; Green, D. W.; Maloney, J. D. *Perry's Chemical Engineer's Handbook*; McGraw−Hill: New York, 1981; Chapter 7.
(41) Reich, L.; Stivala, S. *Elements of Polymer Degradation*; McGraw−Hill: New York, 1971.
(42) Sterling, W. J.; McCoy, B. J. Distribution kinetics of thermolytic macromolecular reactions. *AIChE J.* **2001**, *47*, 2289.
(43) Wang, M.; Smith, J. M.; McCoy, B. J. Continuous kinetics for thermal degradation of polymer in solution. *AIChE J.* **1995**, *41*, 1521.
(44) Kodera, Y.; McCoy, J. B. Distribution kinetics of radical mechanisms: reversible polymer decomposition. *AIChE J.* **1997**, *43*, 3205.
(45) Sezgi, A. N.; Cha, W. S.; Smith, J. M.; McCoy, B. J. Polyethylene pyrolysis: Theory and experiments for molecular-weight-distribution kinetics. *Ind. Eng. Chem. Res.* **1998**, *37*, 2582.
(46) Rice, F. O.; Herzfeld, K. F. The mechanism of some chain reactions. *J. Chem. Phys.* **1939**, *7*, 671.
(47) Gavalas, G. R. The long chain approximation in free radical reaction systems. *Chem. Eng. Sci.* **1966**, *21*, 133.
(48) Nigam, A.; Fake, D. M.; Klein, M. T. Simple approximate rate law for both short- and long-chain Rice Herzfeld kinetics. *AIChE J.* **1994**, *40*, 908.
(49) McCoy, B. J.; Wang, M. Continuous-mixture fragmentation kinetics: particle size reduction and molecular cracking. *Chem. Eng. Sci.* **1994**, *49*, 3773.
(50) Audenaert, W. T. M.; Vermeersch, Y.; Van Hulle, S. W. H.; Dejans, P.; Dumoulin, A.; Nopens, I. Application of a mechanistic UV/hydrogen peroxide model at full-scale: Sensitivity analysis, calibration and performance evaluation. *Chem. Eng. J.* **2011**, *171*, 113.
(51) Xu, B.; Gao, N.-Y.; Cheng, H.; Xia, S.-J.; Rui, M.; Zhao, D.-d. Oxidative degradation of dimethyl phthalate (DMP) by UV/H_2O_2 process. *J. Hazard. Mater.* **2009**, *162*, 954.
(52) Mehrvar, M.; Anderson, W. A.; Moo-Young, M. Photocatalytic degradation of aqueous organic solvents in the presence of hydroxyl radical scavengers. *Int. J. Photoenergy* **2001**, *3*, 187.
(53) Kralik, P.; Kusic, H.; Koprivanac, N.; Loncaric Bozic, A. Degradation of chlorinated hydrocarbons by UV/H_2O_2: The application of experimental design and kinetic modeling approach. *Chem. Eng. J.* **2010**, *158*, 154.

(54) Madras, G.; Chung, G. Y.; Smith, J. M.; McCoy, B. J. Molecular weight effect on the dynamics of polystyrene degradation. *Ind. Eng. Chem. Res.* **1997**, *36*, 2019.
(55) McCoy, B. J.; Madras, G. Degradation kinetics of polymers in solution: dynamics of molecular weight distributions. *AIChE J.* **1997**, *43*, 802.
(56) Madras, G.; Smith, J. M.; McCoy, B. J. Thermal degradation of poly (α-methylstyrene) in solution. *Polym. Degrad. Stab.* **1996**, *52*, 349.
(57) McCoy, B.; Madras, G. Discrete and continuous models for polymerization and depolymerization. *Chem. Eng. Sci.* **2001**, *56*, 2831.
(58) Bird, R. B.; Stewart, W. E.; Lightfoot, E. L. *Transport Phenomena*, Second Edition; John Wiley & Sons: New York, 2002; Chapter 18.
(59) Labas, M. D.; Zalazar, C. S.; Brandi, R. J.; Martín, C. A.; Cassano, A. E. Scaling up of a photoreactor for formic acid degradation employing hydrogen peroxide and UV radiation. *Helv. Chim. Acta* **2002**, *85*, 82.